



## Can the seismic wave attenuation characteristics of various soils be identified using distributed acoustic sensing?

Zhengyu Qian, Dan Zhang\*, Haiyang Liao, Haoyu Wang

School of Earth Sciences and Engineering, Nanjing University, Nanjing 210093, China



### ARTICLE INFO

**Keywords:**

Attenuation characteristics  
Third-party intrusion  
DAS  
Monitoring  
Underground infrastructure

### ABSTRACT

Seismic waves exhibit distinct attenuation characteristics that are contingent upon the medium they traverse. The attenuation characteristics can be employed to monitor engineering activities, such as detecting gas pipeline leaks and third-party intrusions, by the utilization of Distributed Acoustic Sensing (DAS) technology. This study aims to explore the feasibility of identifying the seismic wave attenuation characteristics of different soils using DAS. A circular experimental pit with a diameter of 1 m was designed to measure the responses of various soils. Seismic waves were recorded while propagating through sand and clay under different overlying pressure conditions, encompassing both dry and wet states. The waveform data, collected at various distance from the point of excitation, were analyzed using Power Spectral Density (PSD), Continuous Wavelet Transform (CWT), and quality factor analysis. The energy attenuation amplitude of seismic waves shows an opposite pattern in sand and clay as water content increased. By utilizing the seismic wave attenuation characteristics, it is possible to issue timely warnings for identifying third-party intrusions around urban underground tunnels and pipelines to mitigate potential damage to underground infrastructure.

### 1. Introduction

Seismic wave attenuation is a crucial and extensively researched topic within fields such as geophysics and geotechnical engineering. During the propagation of seismic waves, microstructures within the medium, such as pores and cracks, play a significant role in causing attenuation. Attenuation refers to the gradual loss of energy or decrease in the amplitude of the seismic waves as they travel over a specific distance. As seismic waves encounter these microstructures, the energy of the waves is dispersed and converted into heat due to frictional interactions. This energy dissipation leads to a decrease in the wave's amplitude and intensity. When the waves interact with pores and cracks, the propagation speed and direction may change, as well, resulting in alterations in the shape of the wavefront and the times of arrival. This phenomenon can lead to the distortion of the phase of the seismic waves. The attenuation characteristics of seismic waves vary according to intrinsic properties of the propagation medium, including density, saturation, and uniformity. By utilizing these attenuation characteristics, various events such as pipeline leaks (Muggleton et al., 2020), rock bursts (Wu et al., 2022), as well as the processes like geological storage

of carbon dioxide (Azuma et al., 2014), and underground cavities (Grandjean and Leparoux, 2004) can be monitored. Geophysical method is an effective and widely used non-destructive monitoring method.

Theoretical explanations for seismic wave attenuation can be divided into several categories: (1) When seismic waves propagate through inhomogeneous media, energy attenuation occurs due to scattering effects. Chernov et al. proposed a scalar wave propagation theory, and Knopoff et al. verified the energy attenuation phenomenon of seismic waves propagating in porous media (Hudson and Knopoff, 1989; Varela et al., 1993; Chernov et al., 1961); (2) Based on the assumption of viscoelastic media, various seismic wave energy attenuation models such as Maxwell, Kelvin-Voight, and SLS were developed (Carcione et al., 1988). (3) Based on the assumption that underground media is a biphasic medium, Biot theory (Biot, 1956) and jet flow theory (Dvorkin and Nur, 1993) were developed. Murphy et al. verified that jet flow mechanisms in sediments are the main cause of attenuation of shear wave and compression wave (Murphy, 1982). Therefore, the site media conditions and propagation distance are the main factors affecting the attenuation characteristics of seismic waves.

Distributed Acoustic Sensing (DAS) based on optical fiber (Hartog

\* Corresponding author.

E-mail addresses: [mf21290016@smail.nju.edu.cn](mailto:mf21290016@smail.nju.edu.cn) (Z. Qian), [zhangdan@nju.edu.cn](mailto:zhangdan@nju.edu.cn) (D. Zhang), [haiyangliao@smail.nju.edu.cn](mailto:haiyangliao@smail.nju.edu.cn) (H. Liao), [whynju@smail.nju.edu.cn](mailto:whynju@smail.nju.edu.cn) (H. Wang).

et al., 2013) has emerged as an effective monitoring technique in recent years. The acoustic waves are monitored by calculating the axial strain of optical fibers, and it has been widely used in various fields such as seismic exploration (Mestayer et al., 2011), underground structure imaging (Dou et al., 2017; Zeng et al., 2017, production safety of oil well production safety(Naldrett et al., 2018)), traffic noise monitoring (Lindsey et al., 2020), urban underground space exploration(Jiang et al., 2023), and gas pipeline leakage monitoring(Hussels et al., 2019; Mugleton et al., 2020; Fu et al., 2022). Due to its significant advantages, including long-range capability, anti-interference, cost-effectiveness, and easy deployment, DAS has great potential for application in third-party intrusion warning (Bai et al., 2019; Kim et al., 2022).

To mitigate the risk of third-party intrusions that could potentially compromise critical infrastructures like tunnels and pipelines, a proactive measure is to install optical sensing fibers alongside the infrastructure and to continuously monitor the intrusion events by DAS, ensuring the security and integrity of the infrastructure. As illustrated in Fig. 1, when a third-party intrusion occurs above the optical sensing fiber, such as excavation or drilling, the signal gradually attenuates along the length of the fiber. A specific attenuation pattern appears in the frequency spectrum of each sensing channel. As an intrusion source progresses from the ground surface to deeper positions, the distance between the intrusion source and the optical sensing fiber decreases. The intensity of the intrusion signal received by the optical fiber gradually increases, leading to alterations in the attenuation pattern along the sensing optical fiber. Because the attenuation pattern is closely related to the geological conditions of the site (Biot, 1956; Carcione et al., 1988), intrusion warning zones can be established around the optical fiber by analyzing the attenuation pattern of intrusion signals in different site media and taking into account the local engineering geological conditions. When an intrusion enters the warning zone, a timely alert can be issued.

Typically, the attenuation characteristics of seismic waves has been studied within the range of hundreds of meters to kilometers by using conventional geophysical analysis methods (Rao and Wang, 2015; Bouchaala et al., 2021). However, there are challenges associated with high deployment costs, a limited number of sensors, and the difficulty of achieving real-time monitoring. For third-party intrusion, monitoring is usually conducted within the range of several meters to tens of meters. Research on attenuation at small scales has been relatively ignored, and there is a paucity of studies investigating the potential of utilizing attenuation characteristics for engineering early warnings.

In this paper, a small-scale circular experimental site is established to explore the feasibility of employing DAS for monitoring attenuation characteristics. A simulated third-party intrusion signal is generated at the center of the site, and the propagation of the signal in sand and clay

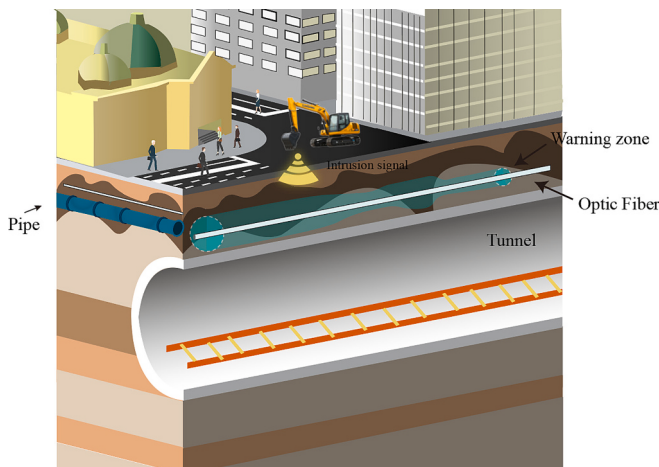


**Fig. 1.** Schematic diagram of third-party intrusion monitoring via optical fiber.

are analyzed. By combining theoretical models, the quality factor is estimated, and attenuation characteristics in different soil are revealed. This research furnishes a theoretical foundation for third-party intrusion monitoring and early warning systems.

## 2. Theoretical principle

### 2.1. Theory of seismic attenuation

According to the theory of viscoelasticity, a uniform non-fully elastic medium will exhibit an absorption phenomenon, resulting in an exponential decrease in the amplitude of seismic waves as they travel through distance, as shown in Eq. (1):

$$A = A_0 e^{-\alpha x} \quad (1)$$

where  $A_0$  is the initial amplitude of the seismic wave,  $A$  is the amplitude after attenuation,  $x$  is the travel distance, and  $\alpha$  is the attenuation factor that characterizes the rate of amplitude decay. Within the seismic frequency band,  $\alpha$  is proportional to frequency  $f$ , which determines the speed of the amplitude attenuation, as shown in Eq. (2):

$$\alpha = \alpha_0 f \quad (2)$$

As a result, Eq. (1) can be rewritten as follows:

$$A = A_0 e^{-\alpha_0 f x} \quad (3)$$

The attenuation factor  $\alpha$  can be expressed as (Xiong et al., 2011):

$$\alpha = -\frac{1}{x} \ln \frac{A(x)}{A_0} = -\frac{1}{A(x)} \frac{dA(x)}{dx} \quad (4)$$

### 2.2. Principle of distributed acoustic sensing

Distributed Acoustic Sensing (DAS) is an optical fiber sensing technology that enables real-time monitoring of vibrations, such as sound, earthquakes, and ambient noise. The DAS system mainly consists of two parts: a demodulator (signal acquisition system) and an optical sensing fiber. The pulsed laser is continuously injected into the optical fiber to collect the backward Rayleigh scattering signal through the demodulator. The axial strain of the fiber can be calculated by measuring the phase difference of the backscattered Rayleigh signals (Karrenbach et al., 2019), as shown in Eq. (5):

$$\Delta\varphi = n_c \frac{2\pi}{\lambda_l} L \varepsilon \quad (5)$$

where  $\varepsilon$  is the axial strain along the fiber,  $\Delta\varphi$  is the phase difference of the backscattered Rayleigh signal,  $L$  is the gauge length,  $n_c$  is the refractive index of the fiber, and  $\lambda_l$  is the wavelength of the laser.

The sensing channel of DAS obtains a waveform as a strain measurement along per unit spatial distance, which is usually referred to as the gauge length. The smaller the gauge length of the fiber, the higher the measurement spatial resolution but the lower the signal-to-noise ratio. The distance between two adjacent midpoint of sensing channels is defined as the channel spacing, and the sensing channels are evenly distributed on the optical fiber with a fixed channel spacing.

## 3. Design of the attenuation experiment

### 3.1. Experimental materials and procedures

#### (1) Experimental materials.

Because of the strong connection between the seismic wave attenuation characteristics and soil types, the experiments involved a comparison between dry and wet conditions for both sand and clay. The particle size distribution curve of the sand is shown in Fig. 2. A single-

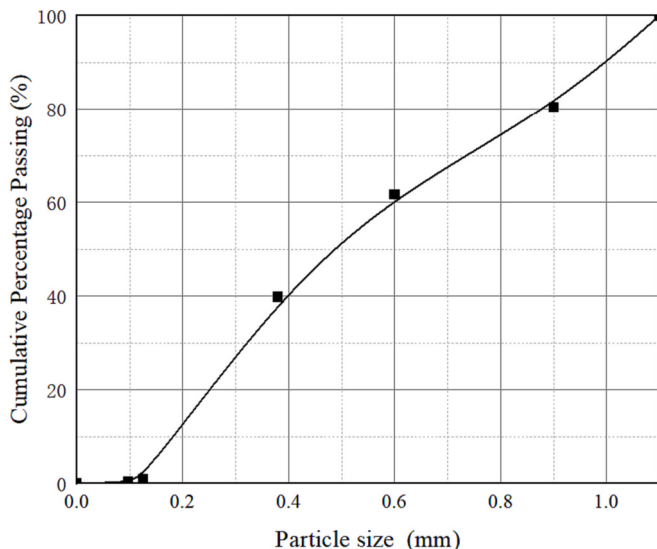


Fig. 2. Gradation curve of sand.

mode optical fiber with diameter of 0.9 mm was used in the experiment. Three sections of optical fibers, each measuring 4 m in length, were used to form optical fiber rings with radii of 10 cm, 20 cm, and 30 cm. These rings are denoted as Fiber A, Fiber B, and Fiber C, as depicted in Fig. 3. A 10 m long segment of free optical fiber was situated between the optical fiber rings. The excitation source utilized was a compaction hammer with capability of reaching a maximum falling height of 30 cm. To simulate different thicknesses of overlying soil above the optical fiber, a total of 17 pieces of 5.1 kg weights and 34 pieces of 2.05 kg weights were incrementally placed on the experimental site. These weights were used to apply different overlying pressure on the soil during the experiment.

## (2) Experimental procedure.

The optical fiber rings were sequentially connected to the DAS demodulator. The sensing channels associated with fiber A, fiber B, and fiber C are as follows: Fiber A corresponds to channels 21–22, Fiber B corresponds to channels 27–28, and Fiber C corresponds to channels 33–34. For both dry and wet sand, as well as clay conditions, three different overlying pressures were applied, namely: (a) no overlying pressure; (b) an overlying pressure of 1.1 kPa; (c) an overlying pressure of 2.21 kPa.

A circular experimental pit was constructed with a diameter of 1 m and a depth of 10 cm. The pit was backfilled with a layer of dry sand, 5 cm in thickness. Then, optical fiber rings, as shown in Fig. 6, were placed on the sand as shown in Fig. 3 and Fig. 4. Afterwards, another layer of dry sand was backfilled in the pit, with a thickness of 5 cm. The compaction hammer was positioned at the center of the optical fiber rings. In each of the three different pressure conditions, the compaction hammer was dropped 12 times respectively from three heights: 10 cm, 20 cm, and 30 cm. The same experiments were conducted on wet sand, dry clay, and wet clay. The water content of the wet sand and wet clay was 10.2% and 23.3%.

## 3.2. Parameter settings and data acquisition

The equipment model of DAS is MS-DAS2000, as shown in Fig. 5. The length of a single data file was 5 s, with a sampling rate of 2 kHz. The channel spacing and gauge length were both 2 m. According to the Nyquist–Shannon sampling theorem, the effective frequency band range that can be captured was 0–1 kHz. The raw data collected is shown in Fig. 7.

## 4. Characteristics of seismic wave attenuation

### 4.1. Variation of attenuation with distance in seismic wave propagation

Each impulse signal excited by the compaction hammer lasts about 0.1 s, as shown in Fig. 7. The average amplitude of all vibrations within 0.1 s was calculated for the 12 signals. These average amplitudes were then compared to determine the maximum average amplitude of the signals received by fiber A, fiber B, and fiber C. Fig. 8 illustrates the maximum average amplitude under the condition of a 2.21 kPa overlying pressure and a 30 cm drop height.

The similarity in the maximum average amplitude obtained by fiber A for both dry and wet sand suggests that the energy of seismic waves propagating within a 10 cm range remains largely consistent. As the propagation distance extends, noticeable discrepancies in amplitude become apparent between the wet and dry conditions for the sand. A similar pattern is observable for dry clay and wet clay. Dry sand, characterized by its loose structure and high porosity, exhibits a decay of approximately 1.75 rads in seismic wave amplitude following a propagation distance of 30 cm. In contrast, wet sand experiences a smaller amplitude decay of approximately 0.6 rads following its propagation over a 30 cm distance. Following a 30 cm distance propagating in dry clay, the reduction in amplitude is approximately 0.5 rads, whereas in

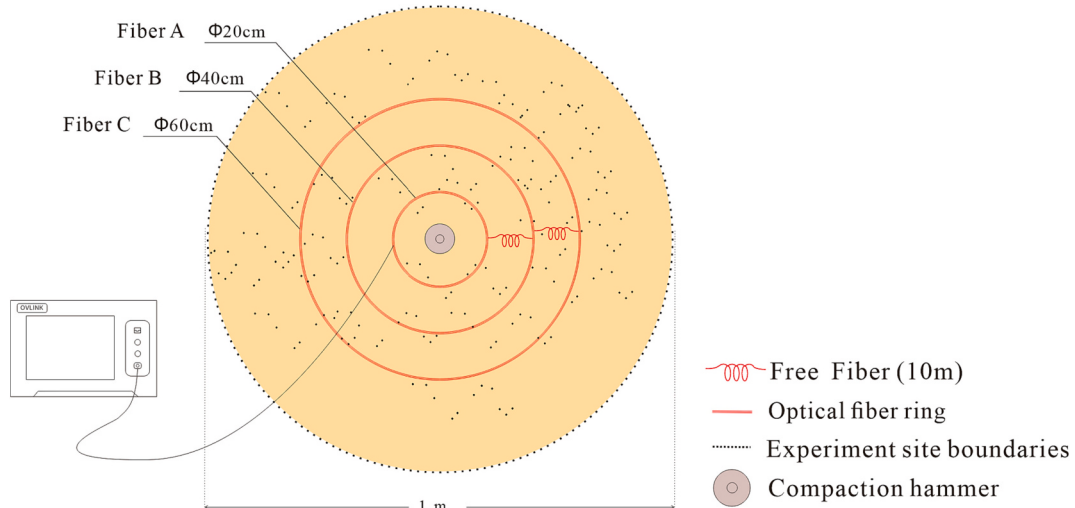


Fig. 3. Plan of the experimental site.

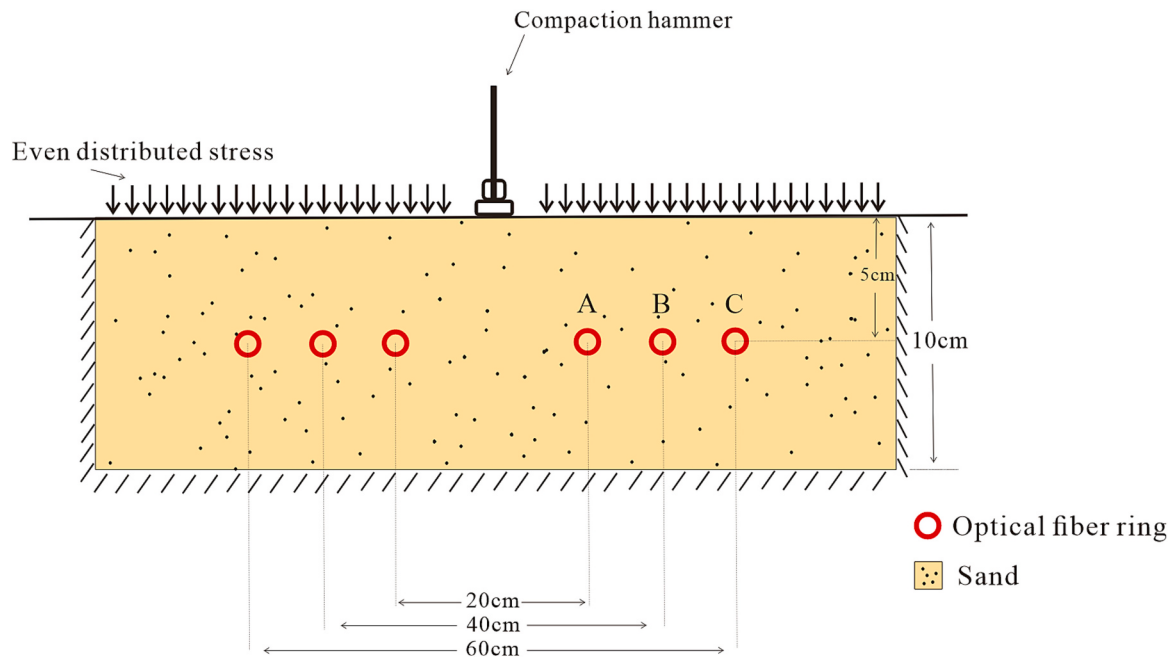


Fig. 4. Profile of the experimental site.



Fig. 5. DAS demodulator.

wet clay, it amounts to about 0.8 rads.

Therefore, it is evident that when the same seismic wave propagates through different soil types, the energy attenuation caused by wet sand is relatively minor, while the energy attenuation resulting from wet clay is larger. The response characteristics of the two soil types to the identical seismic wave are indeed opposite.

#### 4.2. PSD analysis

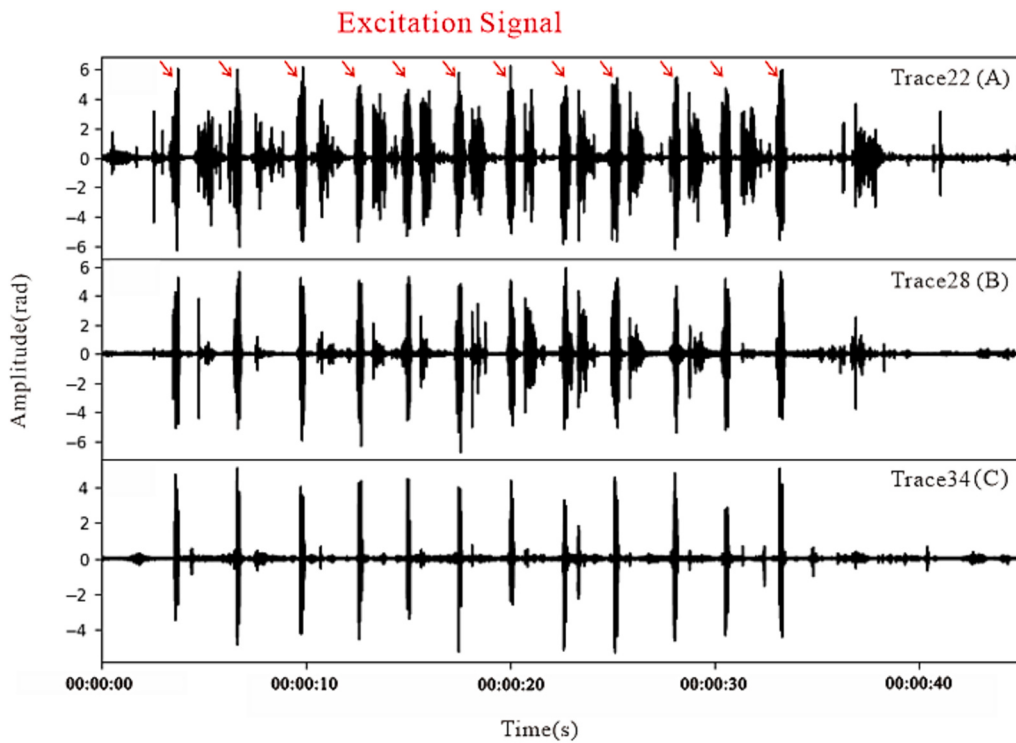
Power Spectral Density (PSD) characterizes the power distribution across different frequency components of a signal, with units of dB/Hz. PSD provides insights into the relative energy of different frequencies, allowing for an intuitive understanding of dominant frequencies in signal and the extent of attenuation across various frequency bands during propagation.

Fig. 9 illustrates the PSD under the conditions of an overlying pressure of 2.21 kPa and a drop height of 30 cm. In Fig. 9(a) and 9(c), the red circles indicate the frequencies corresponding to the maximum energy in dry sand and wet sand, respectively. In dry sand, the frequency

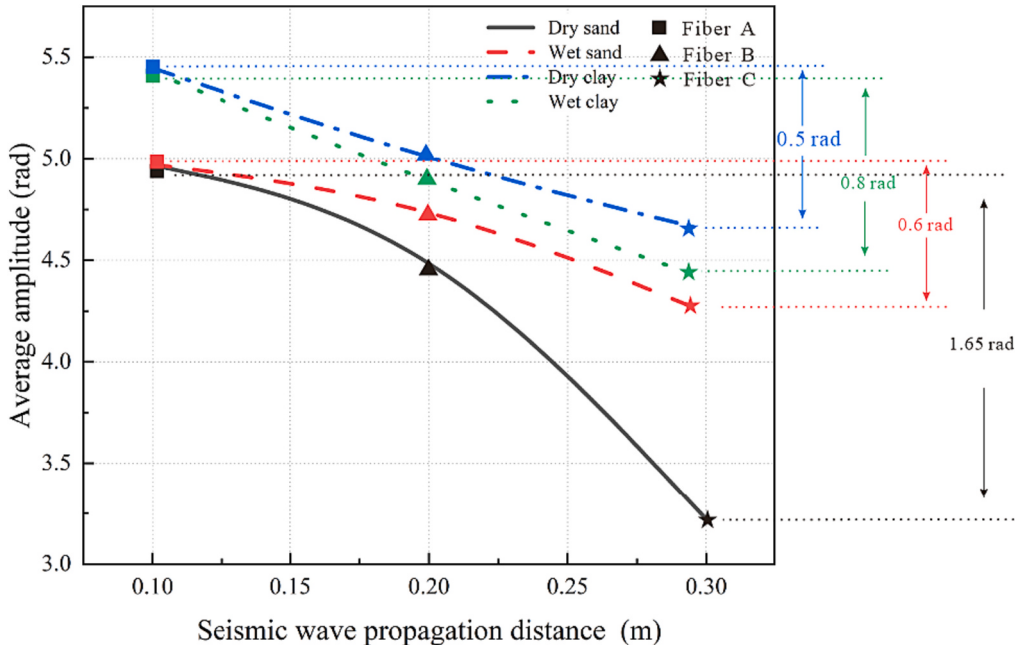


Fig. 6. Optical fiber ring.

corresponding to the maximum energy during propagation is observed at 198 Hz, 181 Hz, and 74 Hz. In wet sand, the frequency corresponding to the maximum energy during propagation is noted at 134 Hz, 130 Hz, and 113 Hz. It is evident that the frequency corresponding to the maximum energy demonstrates a decline as the propagation distance increases, both in dry and wet sand. As depicted in Figs. 9(b) and 9(d), the frequency associated with the maximum energy during propagation is measured at 116 Hz, 64 Hz, and 49 Hz for dry clay, while for wet clay, it is observed at 344 Hz, 145 Hz, and 114 Hz. It is noticeable that the seismic wave propagating through dry clay exhibits a significant reduction in energy as the frequency increases. In Fig. 9, the overall trends of the PSD curves in (a) and (c) are consistent. Within the 100-



**Fig. 7.** Raw data of the 12 compaction hammer drops in wet clay, drop height 30 cm, overlying pressure 2.21 kPa.



**Fig. 8.** Attenuation curve of maximum average amplitude of the vibrations induced by a 30 cm drop under an overlying pressure of 2.21 kPa.

900 Hz range, the energy decreases as the frequency increases, and the frequency corresponding to the maximum energy remains between 100 and 200 Hz, unaffected by changes in moisture content. However, in (d), within the 100–400 Hz range, the energy increases as the frequency increases, and in the 400–900 Hz range, the energy decreases as the frequency increases. There are noticeable changes in the shape of the PSD curve compared to (b) in the case of (d).

The attenuation of signals within the frequency range of 300–700 Hz is more pronounced in dry sand compared to wet sand, as shown in Fig. 9 (a) and (c), indicating that the presence of water in wet sand contributes

to mitigating the rate of energy loss. However, when comparing wet clay to dry clay, it becomes apparent that dry clay shows a smaller degree of attenuation. This observation indicates that the existence of water in viscous soil results in a more substantial level of energy attenuation.

The energy attenuation corresponding to the frequencies of 300, 400, 500, 600, and 700 Hz for all conditions were statistically analyzed, as depicted in Fig. 10. The energy attenuation of the signals propagating in dry sand is stronger than that in wet sand across all conditions. However, in the case of dry clay, the energy attenuation is less significant than that observed in wet clay.

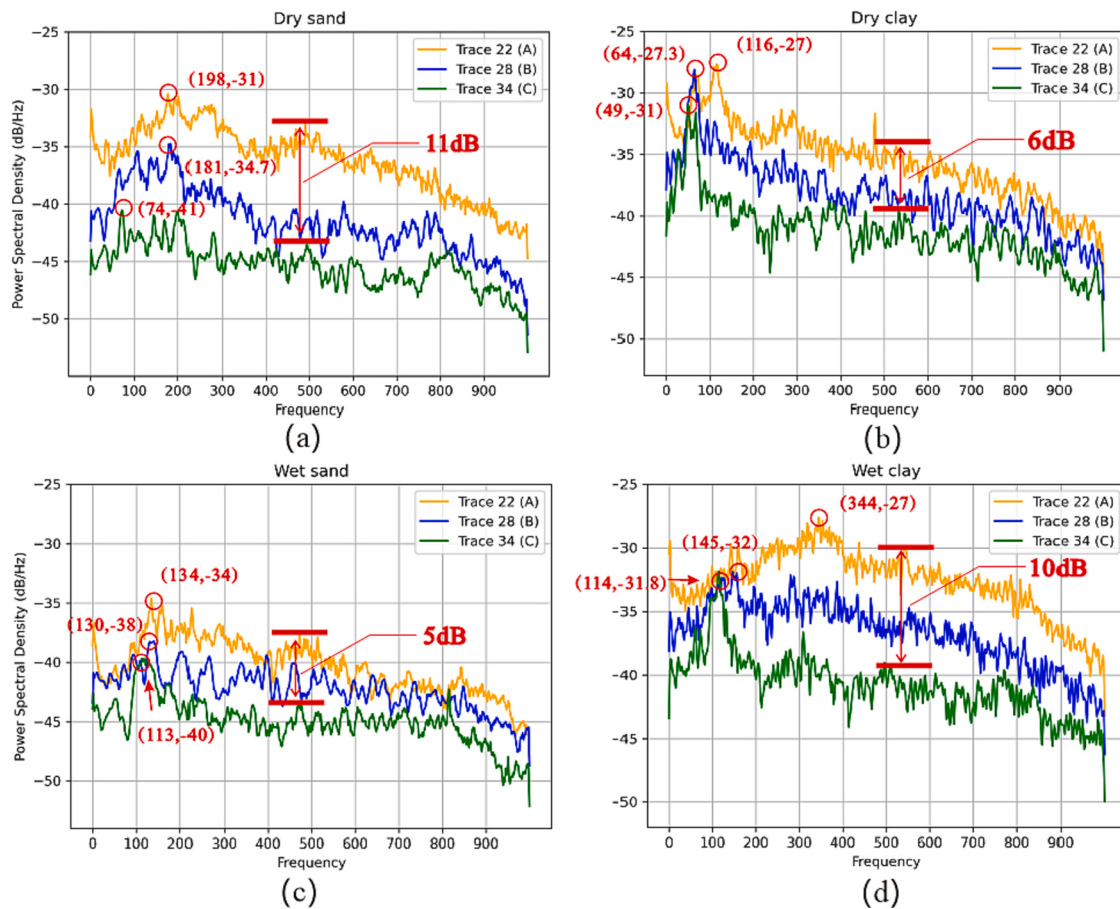


**Fig. 9.** PSD of the vibrations induced by a 30 cm drop under an overlying pressure of 2.21 kPa.

Based on the above analyses, it can be concluded that the attenuation characteristics of the signals differ between sand and clay.

#### 4.3. CWT analysis and attenuation factor calculation

Continuous Wavelet Transform (CWT) is a powerful method for multi-scale time-frequency analysis method commonly employed to examine non-stationary signals. CWT is defined as the inner product of an extended and translated wavelet with the original signal, which can reflect the local characteristics of the signal in the frequency domain with high resolution. Based on this approach, the Morlet wavelet transform were performed on the experimental signals, which enabled the analysis of the energy distribution characteristics across different frequency bands.

Fig. 11 illustrates the CWT outcomes of the signals obtained via fiber A, B, and C. These measurements were conducted under the conditions involving an overlying pressure of 2.21 kPa and a drop height of 30 cm. The bright-colored area in the figure signify a heightened and concentrated energy level, distinguishing them from the areas shaded in darker colors. The extent of the bright-colored area directly correlates with the magnitude of the energy level. In other words, a larger bright-colored area signifies a higher energy level. CWT analysis is performed on an impact signal that occurred between 3.4 s and 3.8 s in the experiment. When the seismic wave propagates distances of 10 cm and 20 cm, the energy received within the low-frequency range (100–200 Hz) is stronger and more concentrated compared to that within the mid-to-high frequency range (200–600 Hz). When the impact signal propagates a distance of 30 cm, it is evident that the bright-colored area within the low-frequency range remains prominent in a large area, while the mid-to-high frequency range appears darker and sparser, indicating a lower

energy level and less concentration of energy. The low-frequency energy is relatively well-preserved and exhibits more concentrated compared to the high-frequency energy as the propagation distance of the impact signal increases. This behavior provides insight into the frequency-dependent attenuation characteristics of seismic wave propagation.

According to Eq. (4), at the location of fiber C, the attenuation factors of the impact signals propagating in dry sand, wet sand, dry clay, and wet clay were calculated to be 1.868, 0.619, 0.795, and 1.043, respectively, when the compaction hammer impact is dropped from a height of 30 cm. This indicates that the different materials (dry sand, wet sand, dry clay, and wet clay) exhibit varying degrees of attenuation, which aligns with the observations made during the signal analysis. The observed variation in attenuation between sand and clay, exhibiting an inverse relationship with water content, harmonizes with the aforementioned rules of seismic wave attenuation. Additionally, the attenuation characteristics follow the same principle: as frequency increases, attenuation also rises. These findings reinforce the understanding of how attenuation behaves within diverse materials and across varying frequency ranges.

#### 5. Estimation of quality factor

In seismology, the intrinsic attenuation of seismic waves due to absorption in geological strata is usually quantitatively described by the Q-factor, which is defined as the energy loss per cycle of the seismic signal and can be expressed as Eq. (6).

$$Q = -\frac{2\pi E}{\Delta E} \quad (6)$$

where  $E$  represents the energy of the seismic signal within one cycle, and

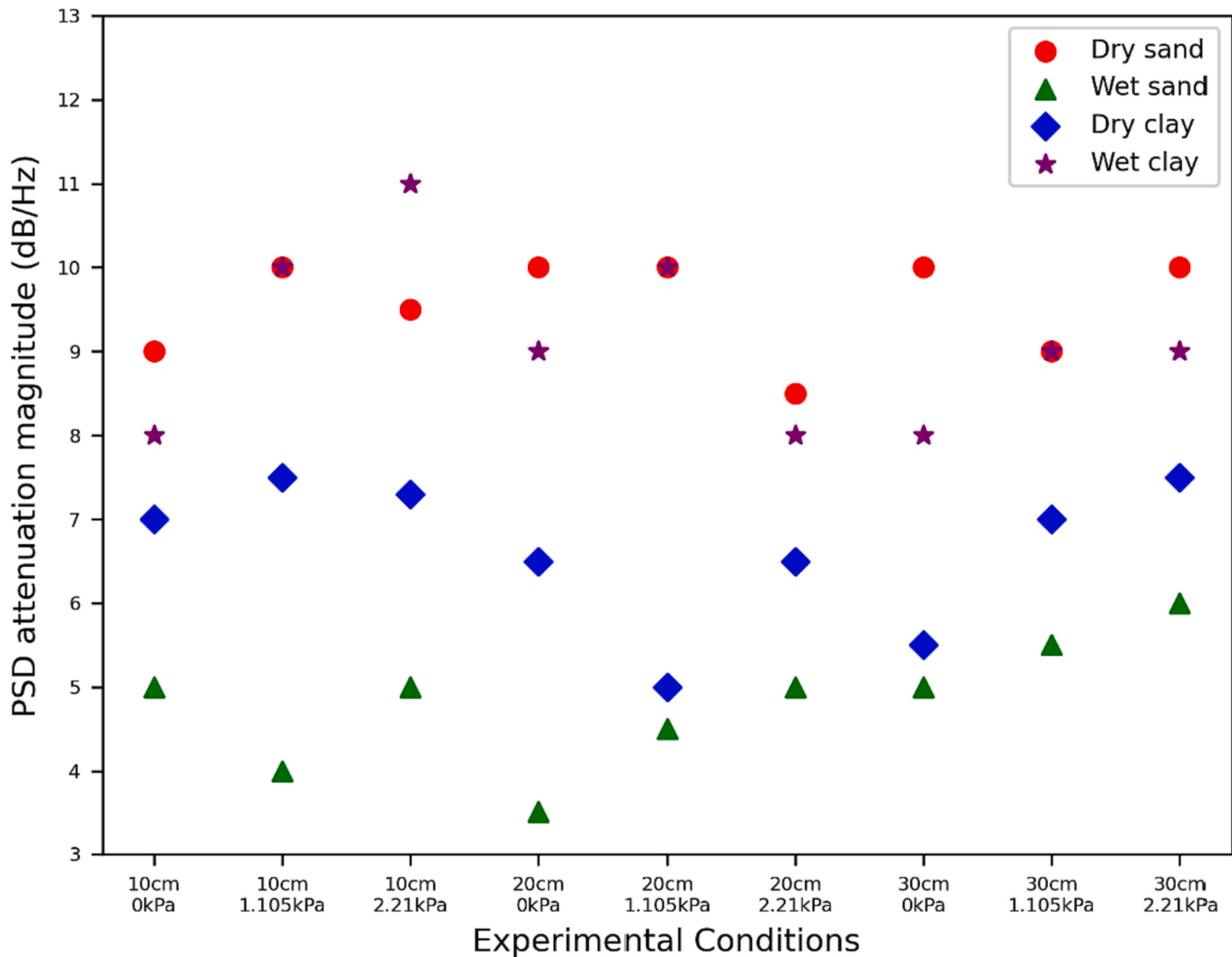


Fig. 10. Energy attenuation values for different conditions.

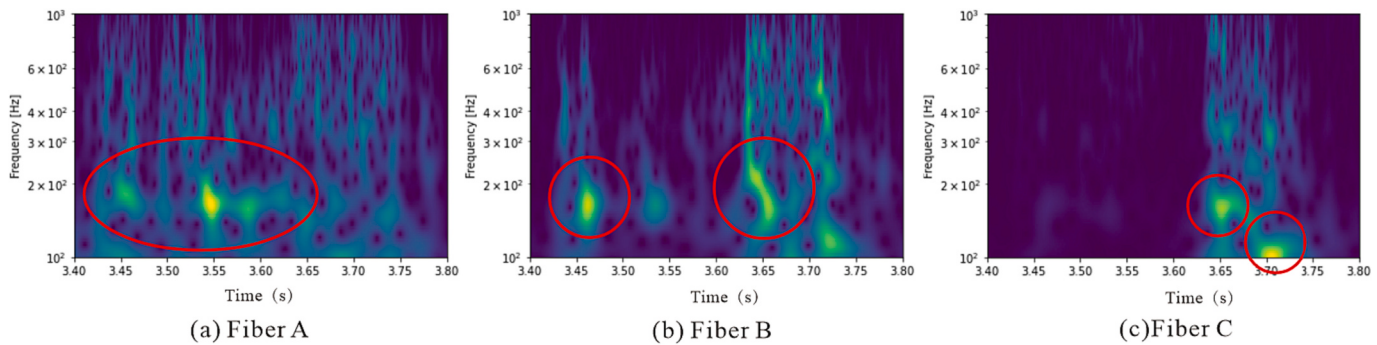


Fig. 11. CWT of the vibration induced by a 30 cm drop under an overlying pressure of 2.21 kPa, wet clay.

$\Delta E$  represents the energy loss of the signal over a certain time period.

$$\frac{dE}{E} = -\frac{2\pi}{TQ} dt \quad (7)$$

$$\frac{dE}{E} = -\frac{2\pi}{TQ} dt \quad (8)$$

$$E = E_0 e^{-\frac{2\pi}{TQ} dt} = E_0 e^{-\frac{2\pi f}{Qv} r} = E_0 e^{-\alpha_E r} \quad (9)$$

where  $E_0$  represents the energy at the seismic source,  $f$  represents the frequency, and  $v$  represents the velocity,  $r$  represents the seismic wave propagation distance.  $\pi f / Qv$  is defined as the energy attenuation coefficient, that is  $\alpha_E$ . The large  $\alpha_E$  is, the more energy is lost and the greater the attenuation experienced by the seismic signal.

Futterman (Futterman, 1962) describes the absorption attenuation of geological formations as a basic property of the formations. There are mainly three categories of methods for estimating Q-factor: (1) Time-domain methods: Amplitude attenuation method (Tyce, 1981),

Wavelet simulation method (Jannsen et al., 1985), and Rise time method (Gladwin and Stacey, 1974), etc.; (2) Frequency-domain methods: Spectral ratio method (Brown, 1978), Centroid frequency shift method (Quan and Harris, 1997), and Peak frequency shift method (Zhang and Ulrych, 2002), etc.; (3) Time-frequency domain methods: Wavelet domain energy attenuation method (Zhao et al., 2004), Estimating Q factor by combining the S-transform with centroid frequency method (Irving and Knight, 2003), etc. The estimation methods for Q-factor lack universality, and the accuracy of the results depends on the quality of seismic data.

Currently, the Spectral Ratio Method (SRM) is a widely used method for Q-factor estimation due to its simplicity, low computational requirements, and ease of practical application. Therefore, in this study, the SRM is adopted to calculate the Q-factor of the experimental soil sample, quantifying the attenuation characteristics of seismic waves in the soil. The amplitude spectrum of seismic waves can be represented as (Kjartansson, 1979):

$$u(r,f) = S(f)G \exp\left(-\frac{\pi f r}{Qv}\right) \quad (10)$$

where  $v$  is the velocity of the stratum,  $S(f)$  is the frequency response of the seismic source,  $G$  is the attenuation term only related to the site conditions, including geometric spreading and transmission losses, and,

$r$  is the propagation distance of the seismic wave.

The logarithm of the ratio of the amplitude spectra at distances  $r_1$  and  $r_2$  can be expressed as:

$$\ln \frac{u(r_2,f)}{u(r_1,f)} = \ln \frac{S_2(f)}{S_1(f)} + \ln \frac{G_2}{G_1} - \frac{\pi f(r_2 - r_1)}{Qv} \quad (11)$$

Assuming the two receiving points have the same source wavelet, the above equation can be simplified as:

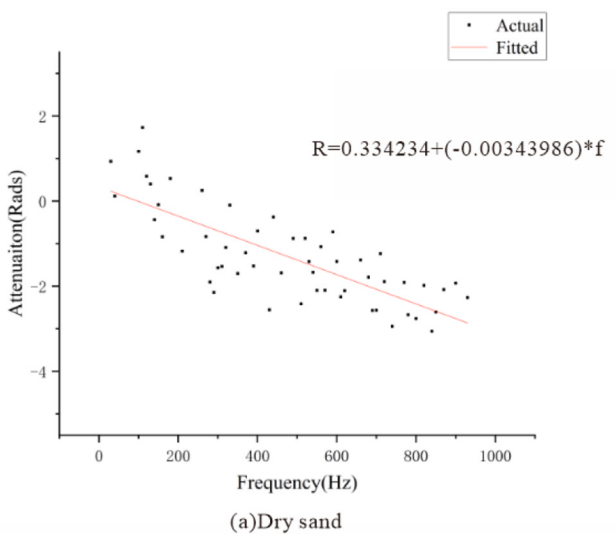
$$R(f) = a - \frac{\pi f \Delta \tau}{Q} \quad (12)$$

where  $\Delta \tau = (r_2 - r_1)/v$ ,  $a$  is a frequency-independent constant, and  $R(f) = \ln[u(r_2,f)/u(r_1,f)]$  is the attenuation function,  $R(f)$  is a linear function of frequency  $f$  with a slope of  $p = -\pi Q^{-1} \Delta t$ , The Q-factor  $Q$  can be obtained by fitting the slope of this expression, that is:

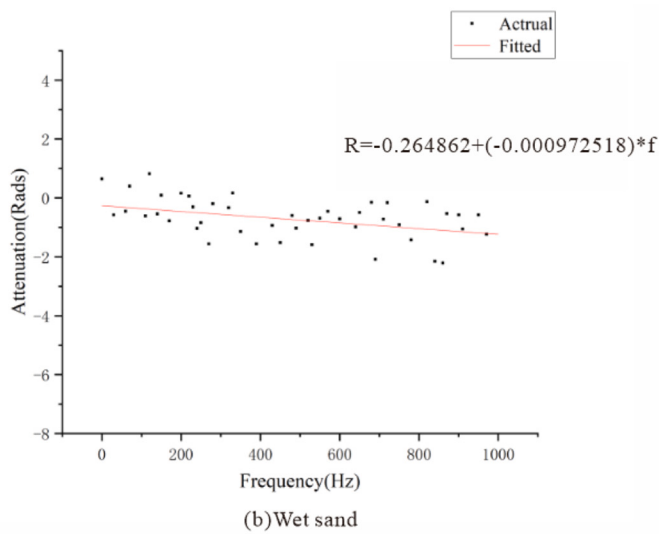
$$Q = -\frac{\pi \Delta t}{p} \quad (13)$$

By fitting the logarithmic relationship between the amplitude spectrum ratio and frequency, the slope  $p = -\pi Q^{-1} \Delta t$  related to  $Q$  is obtained, and then the quality factor can be estimated.

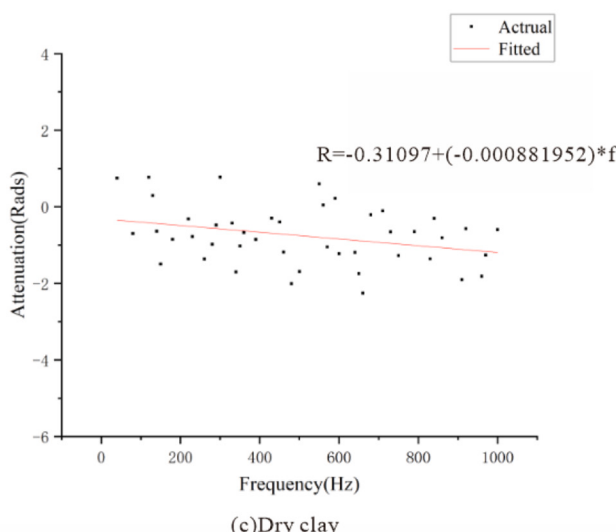
The experimental data collected under the condition of a drop height of 30 cm and an overlying pressure of 2.21 kPa were utilized to fit the



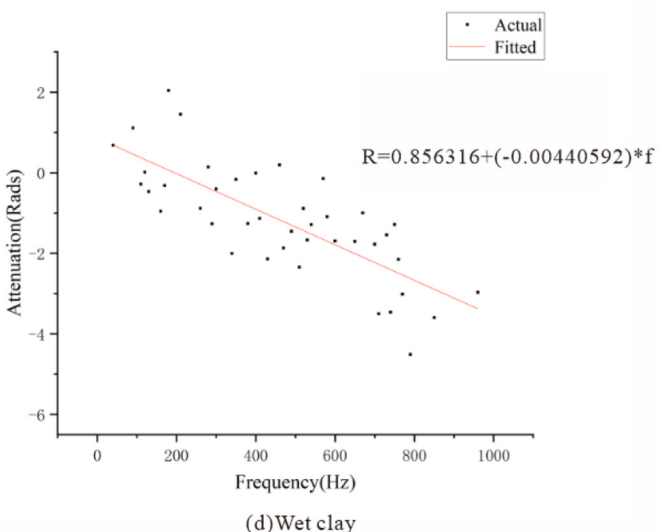
(a) Dry sand



(b) Wet sand



(c) Dry clay



(d) Wet clay

Fig. 12. Attenuation functions for different soil conditions (Fiber A and Fiber C).

attenuation function using the spectral ratio method. The fitting results are shown in Fig. 12. The frequency range of 0–1000 Hz was chosen for analysis, and frequency points were selected at intervals of 10 Hz within this range to calculate the corresponding amplitude spectrum attenuation. After removing some points with large deviations, the attenuation functions were fitted. The corresponding attenuation function slopes for dry sand, wet sand, dry clay, and wet clay were found to be  $-0.00344$ ,  $-0.00097$ ,  $-0.00088$ , and  $-0.00441$ , respectively. The Q-factors are 1.31, 4.62, 2.98, and 0.59, respectively. It was found that the Q-factor of dry sand is smaller than that of wet sand, whereas the Q-factor of dry clay is larger than that of wet clay. In other words, the same seismic signal experiences greater attenuations in sandy soil than in wet sandy soil, whereas the opposite is true in clay. This finding aligns with previous conclusions regarding the attenuation characteristics of these soil types.

## 6. Conclusion

The attenuation patterns of seismic waves are influenced by both the properties of propagation media and the distance of propagation. It is important to reveal the attenuation patterns of seismic waves to establish a scientific basis for engineering monitoring, including the detection of gas pipeline leaks, ground collapses, third-party-intrusion, and other related issues. In this paper, we employ Distributed Acoustic Sensing (DAS) to investigate the propagation and attenuation characteristics of the impact signals in two representative soil types: sand and clay. These characteristics were explored under varying conditions of soil moisture and overlying pressure. The degree of attenuation is quantified by calculating the Q-factor using the spectral ratio method. The main findings and conclusions are summarized follows:

- (1) For both sand and clay, the energy in the low frequency range (0–200 Hz) is dominants, throughout the propagation process, while the energy in the middle and high frequency range (200–800 Hz) is relatively weaker. Only for clay, the proportion of energy in the frequency range of 200–600 Hz increases with the increase in moisture content.
- (2) The influence of moisture on the absorption characteristics of sand and clay is completely opposite. The degree of energy attenuation decreases in wet sand whereas in wet clay, the degree of energy attenuation increases.
- (3) The attenuation pattern of the intrusion signal that occurs every 10 cm during the propagation process in a 30 cm range will have different characteristics, depending on the soil conditions and the propagation distance. In engineering monitoring, when corresponding patterns arise in adjacent sensing channels of accompanying optical cables, it might indicate third-party intrusion. In response, it is possible to establish warning lines within a 10–30 cm perimeter around the optical cable to promptly issue an alert.

By simulating the intrusion signal with the falling signal of a compaction hammer, and combining with DAS, which is a new distributed non-destructive monitoring method, seismic wave signals with obvious attenuation characteristics in both frequency and time domains can be collected. By studying the attenuation characteristics of the signals, solutions for engineering monitoring issues related to disturbance source positioning and third-party intrusion warning in the current geotechnical engineering field can be provided. This has certain research and application value.

## CRediT authorship contribution statement

**Zhengyu Qian:** Writing – review & editing, Writing – original draft.  
**Dan Zhang:** Supervision, Study conception and design, Investigation.  
**Haiyang Liao:** Formal analysis. **Haoyu Wang:** Formal analysis.

## Declaration of competing interest

The authors declare no competing interests.

## Data availability

The authors do not have permission to share data.

## Acknowledgements

This work was supported by the National Natural Science Foundation of China (No. 42077233) and the Natural Science Foundation of Jiangsu Province ((No. BK20231409). We thank Suzhou NanZee Sensing Technology Ltd. for providing the DAS devices.

## References

- Azuma, H., Xue, Z., Matsuoka, T., 2014. Utilization of seismic attenuation in the monitoring of CO<sub>2</sub> geological storage project. Energy Procedia 63, 4216–4223. <https://doi.org/10.1016/j.egypro.2014.11.457>.
- Bai, Y., Xing, J., Xie, F., Liu, S., Li, J., 2019. Detection and identification of external intrusion signals from 33 km optical fiber sensing system based on deep learning. Opt. Fiber Technol. 53, 102060 <https://doi.org/10.1016/j.yofte.2019.102060>.
- Biot, M.A., 1956. Theory of Propagation of Elastic Waves in a Fluid-Saturated Porous Solid. II. Higher Frequency Range. J. Acoust. Soc. Am. 28 (2), 179–191. <https://doi.org/10.1121/1.1908241>.
- Bouchala, F., Ali, M.Y., Matsushima, J., 2021. Compressional and shear wave attenuations from walkway VSP and sonic data in an offshore Abu Dhabi oilfield. Comptes Rendus. Géoscience 353 (1), 337–354. <https://doi.org/10.5802/crgeos.83>.
- Brown, R.J., 1978. Spectral Analysis in Geophysics. J. Franklin Inst. 305 (2), 122–123. [https://doi.org/10.1016/0016-0032\(78\)90008-x](https://doi.org/10.1016/0016-0032(78)90008-x).
- Carcione, J.M., Kosloff, D., Kosloff, R., 1988. Wave propagation simulation in a linear viscoelastic medium. Geophys. J. Int. 95 (3), 597–611. <https://doi.org/10.1111/j.1365-246x.1988.tb06706.x>.
- Chernov, L.A., Silverman, R.A., Sanders, J.L., 1961. Wave Propagation in a Random Medium. J. Appl. Mech. 28 (2), 318–319. <https://doi.org/10.1115/1.3641700>.
- Dou, S., Lindsey, N., Wagner, A.M., Daley, T.M., Freifeld, B., Robertson, M., Peterson, J., Ulrich, C., Martin, E.R., Ajo-Franklin, J.B., 2017. Distributed Acoustic Sensing for Seismic monitoring of the near Surface: a Traffic-Noise Interferometry Case Study. Sci. Rep. 7 (1) <https://doi.org/10.1038/s41598-017-11986-4>.
- Dvorkin, J., Nur, A., 1993. Dynamic poroelasticity: a unified model with the squirt and the Biot mechanisms. Geophysics 58 (4), 524–533. <https://doi.org/10.1190/1.1443435>.
- Fu, S., Zhang, D., Peng, Y., Shi, B., Yedili, N., Ma, Z., 2022. A simulation of gas pipeline leakage monitoring based on distributed acoustic sensing. Meas. Sci. Technol. 33 (9), 095108 <https://doi.org/10.1088/1361-6501/ac7633>.
- Futterman, W.I., 1962. Dispersive body waves. J. Geophys. Res. 67 (13), 5279–5291. <https://doi.org/10.1029/jz067i013p05279>.
- Gladwin, M.T., Stacey, F.D., 1974. Anelastic degradation of acoustic pulses in rock. Phys. Earth Planet. Inter. 8 (4), 332–336. [https://doi.org/10.1016/0031-9201\(74\)90041-7](https://doi.org/10.1016/0031-9201(74)90041-7).
- Grandjean, G., Leparoux, D., 2004. The potential of seismic methods for detecting cavities and buried objects: experimentation at a test site. J. Appl. Geophys. 56 (2), 93–106. <https://doi.org/10.1016/j.jappgeo.2004.04.004>.
- Hartog, H.A., Kotov, O.I., Liokumovich, L.B., 2013. The Optics of distributed Vibration Sensing. Proceedings. <https://doi.org/10.3997/2214-4609.20131301>.
- Hudson, J.A., Knopoff, L., 1989. Predicting the overall Properties of Composite Materials with Small-scale Inclusions or Cracks. Scatte. Attenuat. Seism. Waves, Part II, 551–576. [https://doi.org/10.1007/978-3-0348-6363-6\\_1](https://doi.org/10.1007/978-3-0348-6363-6_1).
- Hussels, M.-T., Chruscicki, S., Arndt, D., Scheider, S., Prager, J., Homann, T., Habib, A.K., 2019. Localization of Transient events Threatening Pipeline Integrity by Fiber-Optic distributed Acoustic Sensing. Sensors 19 (15), 3322. <https://doi.org/10.3390/s19153322>.
- Irving, J.D., Knight, R.J., 2003. Removal of wavelet dispersion from ground-penetrating radar data. Geophysics 68 (3), 960–970. <https://doi.org/10.1190/1.1581068>.
- Jannsen, D., Voss, J., Theilen, F., 1985. Comparison of Methods to Determine Q in Shallow Marine Sediments from Vertical Reflection Seismograms. Geophys. Prospect. 33 (4), 479–497. Portico. <https://doi.org/10.1111/j.1365-2478.1985.tb00762.x>.
- Jiang, W., Lin, J., Liu, B., Zhang, R., Zhang, B., Yang, Z., Gu, Y., 2023. Distributed acoustic sensing for shallow structure imaging using mechanical noise: a case study in Guangzhou, China. J. Appl. Geophys. 215, 105139 <https://doi.org/10.1016/j.jappgeo.2023.105139>.
- Karrenbach, M., Cole, S., Ridge, A., Boone, K., Kahn, D., Rich, J., Silver, K., Langton, D., 2019. Fiber-optic distributed acoustic sensing of microseismicity, strain and temperature during hydraulic fracturing. Geophysics 84 (1), D11–D23. <https://doi.org/10.1190/geo2017-0396.1>.
- Kim, H., Lee, J., Jung, H., Kim, Y.H., Kwon, J.H., Ki, S.D., Kim, M.J., 2022. Development of Long-perimeter Intrusion Detection System aided by Deep Learning-based distributed Fiber-optic Acoustic-vibration Sensing Technology. J. Sens. Sci. Technol. 31 (1), 24–30. <https://doi.org/10.46670/jsst.2022.31.1.24>.

- Kjartansson, E., 1979. Constant Q-wave propagation and attenuation. *J. Geophys. Res. Solid Earth* 84 (B9), 4737–4748. Portico. <https://doi.org/10.1029/jb084ib09p04737>.
- Lindsey, N.J., Yuan, S., Lellouch, A., Gualtieri, L., Lecocq, T., Biondi, B., 2020. City-Scale Dark Fiber DAS Measurements of Infrastructure Use during the COVID-19 Pandemic. *Geophys. Res. Lett.* 47 (16), Portico. <https://doi.org/10.1029/2020gl089931>.
- Mestayer, J., Cox, B., Wills, P., Kiyashchenko, D., Lopez, J., Costello, M., Bourne, S., Ugueto, G., Lupton, R., Solano, G., Hill, D., Lewis, A., 2011. Field trials of distributed acoustic sensing for geophysical monitoring. *SEG Techn. Prog. Expand. Abstr.* 2011 <https://doi.org/10.1190/1.3628095>.
- Muggleton, J.M., Hunt, R., Rustighi, E., Lees, G., Pearce, A., 2020. Gas pipeline leak noise measurements using optical fibre distributed acoustic sensing. *J. Nat. Gas Sci. Eng.* 78, 103293 <https://doi.org/10.1016/j.jngse.2020.103293>.
- Murphy, W.F., 1982. Effects of partial water saturation on attenuation in Massilon sandstone and Vycor porous glass. *J. Acoust. Soc. Am.* 71 (6), 1458–1468. <https://doi.org/10.1121/1.387843>.
- Naldrett, G., Cerrahoglu, C., Mahue, V., 2018. Production monitoring using Next-Generation distributed Sensing Systems. *Petrophys. – SPWLA J. Format. Evaluat. Reserv. Descript.* 59 (4), 496–510. <https://doi.org/10.30632/pjv59v4-2018a5>.
- Quan, Y., Harris, J.M., 1997. Seismic attenuation tomography using the frequency shift method. *Geophysics* 62 (3), 895–905. <https://doi.org/10.1190/1.1444197>.
- Rao, Y., Wang, Y., 2015. Seismic signatures of carbonate caves affected by near-surface absorptions. *J. Geophys. Eng.* 12 (6), 1015–1023. <https://doi.org/10.1088/1742-2132/12/6/1015>.
- Tyce, R.C., 1981. Estimating acoustic attenuation from a quantitative seismic profiler. *Geophysics* 46 (10), 1364–1378. <https://doi.org/10.1190/1.1441144>.
- Varela, C.L., Rosa, A.L.R., Ulrych, T.J., 1993. Modeling of attenuation and dispersion. *Geophysics* 58 (8), 1167–1173. <https://doi.org/10.1190/1.1443500>.
- Wu, J., Liu, Q., Zhang, X., Zhou, C., Yin, X., Xie, W., Liang, X., Huang, J., 2022. Attenuation characteristics of impact-induced seismic wave in deep tunnels: an in situ investigation based on pendulum impact test. *J. Rock Mech. Geotech. Eng.* 14 (2), 494–504. <https://doi.org/10.1016/j.jrmge.2021.12.005>.
- Xiong, X.-J., He, X.-L., Pu, Y., He, Z.-H., Lin, K., 2011. High-precision frequency attenuation analysis and its application. *Appl. Geophys.* 8 (4), 337–343. <https://doi.org/10.1007/s11770-011-0302-4>.
- Zeng, X., Lancelle, C., Thurber, C., Fratta, D., Wang, H., Lord, N., Chalari, A., Clarke, A., 2017. Properties of Noise Cross-Correlation Functions Obtained from a distributed Acoustic Sensing Array at Garner Valley, California. *Bull. Seismol. Soc. Am.* 107 (2), 603–610. <https://doi.org/10.1785/0120160168>.
- Zhang, C., Ulrych, T.J., 2002. Estimation of quality factors from CMP records. *Geophysics* 67 (5), 1542–1547. <https://doi.org/10.1190/1.1512799>.
- Zhao, W., Li, H., Cao, H., Yao, F., 2004. Attenuation characteristics of seismic waves in the wavelet domain and the detection of gas. *SEG Techn. Prog. Expand. Abstr.* 2004 <https://doi.org/10.1190/1.1845135>.